PAN Confined Polymerization in Mesoporous Hexagonal *p*-Phenylenesilica with Crystalline-like Order in their Walls and Thermal Transformation of the Nanostructured Material

Angiolina Comotti,[†] Silvia Bracco,[†,*] Mario Beretta,[†] Jacopo Perego,[†] Mauro Gemmi[‡] and Piero Sozzani[†,*]

[†] Department of Materials Science, University of Milano Bicocca, Via R. Cozzi 55, 20125 Milan, Italy

[‡] Inst. Italiano Tecnol., Center Nanotechnol Innovat NEST, Piazza San Silvestro 12, I-56127 Pisa, Italy

KEYWORDS. Periodic Mesoporous Organosilicas · Confined Polymerization · Nanostructures · Ladder polymers

ABSTRACT: Mesoporous ordered *p*-phenylene silica provided an ideal channel-like reaction vessel for the polymerization of acrylonitrile by a confined radical process. The prismatic nanospaces, permeable to monomers in the hybrid covalent framework, exhibit a hexagonal cross-section of 5 nm and faces decorated with alternating organic/inorganic siloxane layers. The resulting high-molecular-mass PAN polymer fills the channels at high yield and forms an ordered nanostructure of polymer nanobundles enclosed in the hybrid matrix. During the transformation of PAN into rigid polyconjugated and, eventually, into condensed polyaromatic carbon nanofibers, the periodic architecture is retained up to high temperatures. The matrix evolves simultaneously showing a thermal condensation of the aromatic layers and cleavage of carbon-silicon bonds: this gives rise to graphitic-carbon/silica nanocomposites containing hyper-oxydrilated silica nanoparticles, which are thus generated *in situ* under the architecture constraints. The 3D hexagonal mesostructure survives in the carbonaceous material, but with homogeneous shrinkage at such extreme temperatures. Several solid-state techniques, such as variable temperature synchrotron XRD, TEM and 1D/2D multinuclear MAS NMR combined with ^{13}C-labelling, allowed us to understand the chemical and periodic order of the nanostructured material with confined polymer-chains and an intimacy between host and guest nanophases. The exploitation of porous materials, of high capacity and a hybrid nature, for polymerization in the confined state, followed by high temperature treatments, allowed us to achieve unique and sophisticated, but still precisely fabricated, nanostructures, thus paving the way for the construction of fine-tuned electronic and light-harvesting hybrid nanostructures.

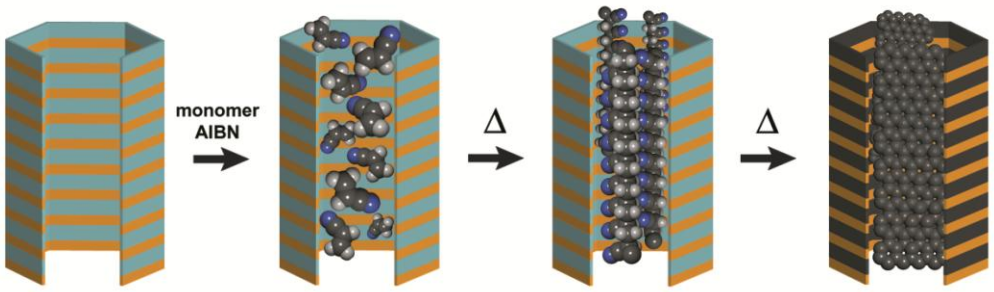

INTRODUCTION

Polymerization in nanospaces has recently attracted considerable interest as a novel route to fabricating functional materials[1] and to control polymer architecture over hierarchical levels, such as microstructure, morphology and nano- and micro-object generation, thus gaining access to properties that are distinctly different from those of the corresponding bulk phases.[2] In this context, mesoporous materials have been used as a valid platform for the formation of nanostructured materials, nanocomposites and interpenetrated polymers.[3] Furthermore, mesoporous silicas have been useful in hard templating processes as starting mold for the formation of mesoporous carbons or polymeric micro-objects, giving the unique opportunity to transfer the regular mesostructure from one material to the other.[4]

Mesoporous organosilicas deserve particular attention because they join the stiffness of inorganic structures with the wide applica-

tion fields of organic chemistry. These materials can be realized by the post synthetic grafting of functional organic groups on silica mesopores, or by co-condensation of silanes and organosilanes in template synthesis.[5] However, with these methods there is the difficulty of homogeneous distribution and the high-loading of organic moieties, and this represents a severe limitation. New hybrid and mesoporous materials obtained by homocondensation of bis-substituted organosilanes could achieve the goals.[6] Additionally, the bis-substituted organosilane can self-organize in an ordered way, resulting in crystal-like channel walls, called periodic mesoporous organosilica materials (PMOs).[7] Indeed, the presence of different organic moieties in PMO frameworks deeply influences the chemical and physical properties of such materials, and new functional materials such as optical systems for light harvesting and photonics,[8] materials for drug-delivery in pharmaceutical applications[9], scaffolds for nanocomposites in medical and biological research[10] and molecular rotor systems have been discovered.[11] Nevertheless, despite the large number of applications confined-polymerization is a novelty in the field of mesoporous organosilicas with crystalline-like order in their walls.

Here we propose the use of ordered mesoporous *p*-phenylenesilicas containing nanochannels, lined with aromatic rings as reaction vessels, for *in situ* solid-state polymerization and the fabrication of novel nanostructured materials (Scheme 1). The framework topology provides parallel and independent mesochannels that are prone to efficiently capture a large amount of monomer that can easily polymerize, forming aligned polymer chains or nanofibers within the hybrid framework. Acrylonitrile was successfully polymerized within the channels, fabricating an organosilica-polymer nanocomposite endowed with a hierarchical order: aligned PAN chains in each hexagonal mesochannel and an ordered array of PAN bundles in the hybrid hexagonal framework.

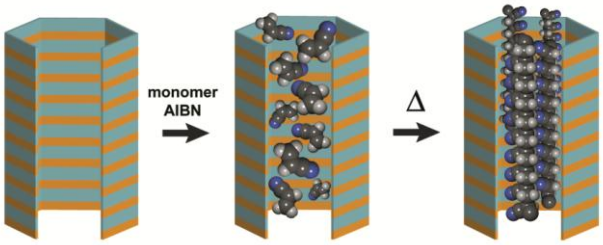

Scheme 1. Schematic representation of the in situ polymerization in mesoporous ordered organosilica.

The thermal transformation of the polyacrylonitrile (PAN) and of host organic moieties in a non-oxidative atmosphere led to the formation of a nanocomposite with graphitic-like carbon structures. Both the *in situ* polymerization and the thermal evolution of the matrix/polymer nanocomposite until graphitization was studied by combining techniques such as N_2 adsorption isotherms, calorimetric analysis, solid state NMR of ^{13}C-enriched polyacrylonitrile and TEM. Powder X-ray diffraction using synchrotron radiation was applied to follow, *in situ*, the mesoscale and molecular order evolution of both the empty matrix and the nanocomposite from 300K to 1350K, while multinuclear ^{1}H-^{13}C and ^{1}H-^{29}Si SS NMR highlighted the chemical species at distinct steps and demonstrated the polymer inclusion in the *p*-phenylenesiloxane mesochannels. Transmission electronic microscopy revealed the pore-channel structural modifications after thermal evolution.

EXPERIMENTAL SECTION

Synthesis. *p*-Phenylenesilica material (PPS) was prepared by a template synthesis in which the hybrid building blocks, 1,4-bis(triethoxysilyl)benzene (BTEB) self-organizes around amphiphilic molecules of octadecyltrimethylammonium bromide (ODTMA) in a sodium hydroxide (NaOH) aqueous solution. The molar ratios of the reactants are the following: 0.96:1.00:4.03:559.23 C18TMABr/BTEB/NaOH/H_2O. ODTMA was dissolved in the sodium hydroxide aqueous solution at 60-70 °C to ensure the complete dissolution, and then BTEB was added dropwise to the solution under vigorous stirring at room temperature. The mixtures were treated ultrasonically for 20 min to improve dispersion, stirred at room temperature for 20 h, and then kept at 95 °C for 20 h under static conditions. The white precipitates were recovered by filtration and dried to yield the *p*-phenylenesilica material containing the surfactant molecules. The surfactant was removed by stirring 1 g of powder in 250 mL of ethanol and 9 g of 36% hydrochloride aqueous. The complete surfactant removal was confirmed by DSC and IR-ATR measurements. In IR-ATR spectra it is clearly visible the loss of signals at 2850 and 2920 cm^{-1} typical of long-chain organic ammonium salts, whilst in DSC traces no transition at about 40-50 °C associated to the surfactant micellar phase was observed. A solution of AIBN (azobisisobutyronitrile, 0.7%) in distilled acrylonitrile was transferred over the evacuated mesoporous organosilica. The sample underwent freeze and thaw cycles and was left in the dark at 273K for 4 days. Excess solution was filtered off and the collected sample was heated for 4 hours at 373K to activate the polymerization. The formation of the mesostructured material (PPS-PAN) was checked by DSC calorimetric analysis from the exotherm profile in the range 443-573K. Polymerization in the *p*-phenylenesilica using a monomer mixture containing a 20% wt ^{13}C-enriched monomer on nitrile carbon was performed to yield the labelled nanocomposite (PPS-^{13}C-PAN). If present, minor amounts of excess polymer were removed by washing in DMSO/MeOH. Nanocomposites with excess polymer (PPS-*exc*-PAN) were prepared with increasing monomer-to-matrix ratios avoiding removal of monomer or excess polymer.

Thermal treatment of the organosilica matrix and the mesostructured material. The empty PPS matrix and PPS-PAN were heated as follows. First, the samples were gradually heated (100 K/hour) under N_2 atmosphere up to 573 K, then they were kept at 573K for 30 minutes. The colour of samples changed from white to yellow and finally to brown-orange. The PPS and PPS-PAN samples were heated under argon at 1350 K for 6h for the carbonization process (denoted, g-PPS and g-PPS-PAN, respectively). The samples appeared as a black powder. In the *g*-PPS-PAN, the amount of nitrogen was measured to be 4% as normalized to PAN content by elemental analysis.

Adsorption isotherms. N_2 adsorption measurements have been performed on a 2050 ASAP Micromeritics instrument. Data were collected from 0.01 to 0.98 P/P_0 pressure with a delay time of 5 seconds. Surface area was calculated using the Brunauer, Emmet, and Teller (BET) model. The pore-size distributions were evaluated following the method developed by Barret, Joyner, and Halenda (BJH model) for cylindrical pores and by nonlinear density functional theory (DFT) analysis. No hysteresis was apparent throughout the entire pressure range. The samples were evacuated at 160°C

overnight, except for the PPS-PAN compound, that was heated at 120°C to avoid polyacrilonitrile cyclization.

Calorimetric analysis. TGA and DCS analysis were on a Mettler-Toledo TGA/DSC 1 Star^e system and a Mettler-Toledo DSC 1 Star^e system. TGA were performed in air from room temperature to 900°C at 10°C/min.

Solution and solid state NMR. ^{1}H and ^{13}C NMR experiments on extracted polymer were performed on a 400 MHz Varian instrument. The polymer was dissolved in deuterated DMSO and analysis were conducted at 80°C. The solid-state NMR spectra were run at 75.5 MHz for ^{13}C and at 59.6 MHz for ^{29}Si on a Bruker Avance 300 instrument operating at a static field of 7.04 T equipped with high-power amplifiers (1 kW) and a 4 mm double resonance MAS probe. The samples were spun at a spinning speed of 15 kHz, and ramped-amplitude cross-polarization (RAMP–CP) transfer of magnetization was applied. The 90° pulse for protons was 2.9 μs (86 kHz). ^{13}C and ^{29}Si cross polarization (CP) magic angle spinning (MAS) experiments were performed using a recycle delay of 6 s and a contact time of 2 and 8 ms, respectively. Quantitative fully relaxed ^{13}C and ^{29}Si single-pulse excitation (SPE) experiments with dipolar decoupling from hydrogen were run using recycle delay of 60/150 s. Phase-modulated Lee–Goldburg (PMLG) heteronuclear ^{1}H–^{13}C and ^{1}H–^{29}Si correlation (HETCOR) experiments combined with fast MAS allowed the recording of 2-D spectra with high resolution both in the hydrogen and rare-nuclei dimensions. PMLG ^{1}H–^{13}C and ^{1}H–^{29}Si HETCOR spectra were run with an LG period of 18.9 μs. Quadrature detection in t_1 was achieved using the time proportional phase increments (TPPI) method. Efficient transfer of magnetization to the carbon nuclei was performed applying a RAMP–CP sequence. CP times from 0.5, 2, 5 and 8 ms were applied. Carbon and silicon signals were acquired during t_2 under proton decoupling applying a two-pulse phase modulation (TPPM) scheme. Quantitative ^{1}H MAS NMR measurements were performed with a Bruker Avance III 600 MHz instrument operating at 14.1 T, using a recycle delay of 20 s. A MAS Bruker probe head was used with 2.5 mm ZrO_2 rotors spinning at 33 kHz.

Synchrotron X-ray diffraction. In-situ synchrotron X-ray powder diffraction experiments were performed at the European Synchrotron Radiation Facility (ESRF) in Grenoble on the BeamLine Gilda-BM08, with a Debye-Scherrer type diffractometer equipped with a gas handling system.34 The radiation wavelength λ of the incident X-rays was 0.78 Å; the 2θ range was from 0.8° to 15°. The powder samples were loaded into a glass capillary, inner diameter 0.8 mm. The powder X-ray diffraction patterns were performed at variable temperature, from room temperature to 1270 K at a heating rate of 10 K/min.

Powder X-ray diffraction. XRD experiments were performed with a Bruker D8 Advance Diffractometer ($Cu_{K\alpha}$ radiation) instrument. Data have been collected from 1.5 to 60.0 2θ degrees with a step of 0.2 degrees and 20 seconds of step time.

Transmission Electron Microscopy. The TEM images were obtained using a JEOL JEM-3010 with *V*) 300 kV. Laser light diffraction analyses were performed using Tri-laser Microtrac S3500 apparatus.

Raman Spectroscopy. Raman measurements were carried out using a Labra Jobin-Yvon spectrometer in conjunction with 488 nm Ar laser excitation source at room temperature. Microwave conductivity measurements were performed exploiting an Agilent network analyzer, working in the range 500 MHz – 50 GHz, equipped with a rectangular waveguide cavity resonator and a cylindrical performance probe of 9.5 mm in diameter.

RESULTS AND DISCUSSION

Polymerization in *p*-phenylenesilica nanochannels. The process of *in situ* polymerization was performed in a porous covalent architecture that guarantees permanent porosity and robustness, even under severe conditions. The matrix of choice was the hybrid mesoporous *p*-phenylenesilica PPS endowed with nanochannels and crystal-like regularity in the channel walls, as shown by TEM and XRD (Figure 1a,b and d). A large surface area and porosity are essential prerequisites for the use of this ordered material as a polymerization vessel; the accessibility and easy impregnation of the pores from a fluid phase after short diffusion times is another advantageous condition of permanently porous materials, allowing for massive monomer diffusion. Indeed, the open mesoporosity of the selected host matrix and the potential accessibility of the pores to monomers was demonstrated by the N_2 adsorption isotherm at 77K, which exhibits a type-IV curve and indicates a surface area of 725 m^2/g by BET analysis, a narrow pore size distribution centered at 38 Å by BJH and NLDFT methods as well as a significant pore volume capacity of 0.77 cm^3/g (Figure 1d). The periodic mesoporous *p*-phenylenesilica displays high structural order on both the molecular and meso scale, as demonstrated by powder X-ray diffraction. An intense peak at 47.7 Å *d*-spacing, typical of hexagonal structures with parallel channels, and three additional peaks at 7.6, 3.8 and 2.5 Å, related to the ordered *p*-phenylene moieties along the channel walls, were detected. Indeed, PPS channel walls are composed by aligned and ordered aromatic rings pivoted between two siloxane layers, as reported in Figure 1c. The fact that the organic units are homogenously incorporated in the 3D crystalline structure, and exposed to the empty channel, allowed us to realize an unprecedented polymerization process that enabled the fabrication of novel matrix-polymer nanostructured materials with polymer chains aligned parallel to the surrounding host aromatic groups.

The porous material was soaked with acrylonitrile monomer containing the radical initiator 2,2′-azobisisobutyronitrile and, after removal of the monomer excess, the sample was heated at 100°C for 4 hours under inert atmosphere for the polymerization process. In the nanostructured PPS-PAN we observed a drastic reduction of both surface area and pore volume, to 95 m^2/g and 0.18 cm^3/g, respectively, whilst no changes in XRD *d*-spacing peaks were observed. The diffraction peak at *d*=47.7 Å showed a decreased intensity caused by reduced electron contrast between the walls and the inner part of channels owing to the polymer occupying the channels (Figure 1e). This is the first proof that the polymerization process did not disrupt the host matrix, and the polyacrylonitrile was formed inside the nanochannels.

The polymer content was determined by thermogravimetric analysis: an overall 60% weight loss of the nanocomposite corresponding to the degradation of both the polymer and the organic phase of the

host matrix was measured (Figure 1f).[12] Comparison with the TGA trace of the empty matrix, showing a weight loss of 40% above 600°C, enabled the estimation of the polymer/host ratio as being 0.56 g/g in the nanocomposite. Independent information concerning the composition of the nanostructured material was obtained from a ^{13}C MAS NMR spectrum, recorded with a long recycle delay for a quantitative analysis (Supporting Information). This analysis highlights the formation of the polymer: the characteristic signals of poly(acrylonitrile) and host matrix were observed selectively. From the integrals of the peaks, the polymer/host ratio was established to be 0.59 g/g. The content of included polymer in the hybrid matrix is high compared to that of confined polymerization in microporous materials[2b] and corresponds to a pore-filling of about 70% of the pore volume, based on bulk PAN density (d=1.15 g/cm^3) and the total free volume of PPS. From the NMR analysis it is apparent that the polymerization reaction went to completion as no monomer signals in ^1H or ^{13}C spectra were detected (Supporting Information).

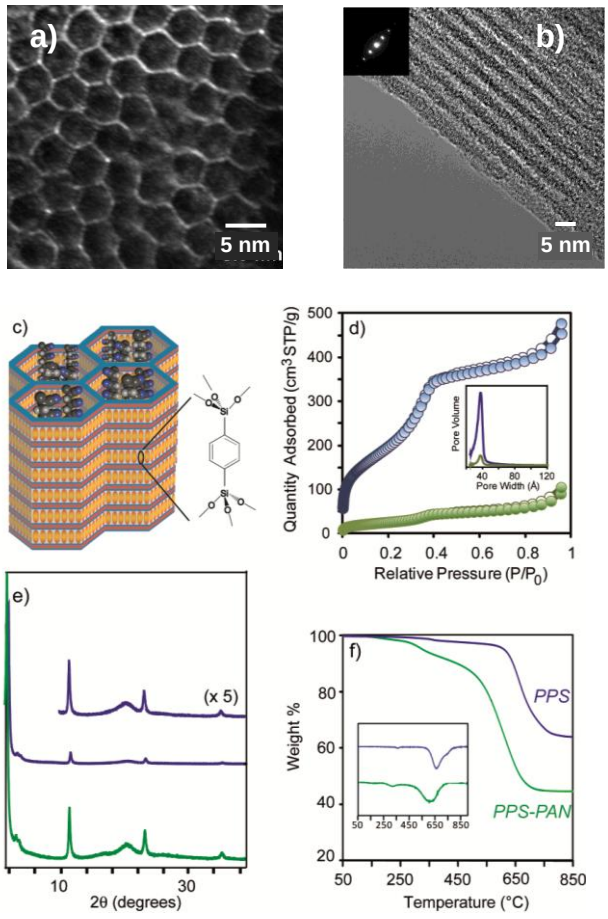

Figure 1. HRTEM images of empty PPS viewed along the channel axis (a) and perpendicular to the channel axis (b). In the inset the electron diffraction pattern is reported. c) Schematic representation of the mesoporous organosilica with confined PAN. d) N_2 adsorption isotherms at 77K; e) Powder X-ray diffraction and f) TGA traces. Blue and green colors correspond to PPS and PPS-PAN, respectively.

The polyacrylonitrile, extracted from the host matrix by etching the nanocomposite in HF solution, exhibited a molecular mass as high as 70 kDa, calculated by viscometry in DMSO and applying the Mark-Houwink equation (K=0.0321 mLg^{-1} and a=0.75). The polyacrilonitrile resulted as being atactic (see ^1H and ^{13}C NMR spectra in Supporting Information), as expected by the radical polymerization in the host channels with a large cross-section of 4 nm.

Multidimensional MAS NMR spectra of the PPS-PAN nanocomposite clearly proved the intimacy of the polymer chains with the hybrid host, and the effective inclusion of the polymer chains in the mesochannels. Indeed, fast magic-angle spinning 2D ^1H–^{13}C and ^1H–^{29}Si HETCOR NMR spectra (Figure 2), performed under Lee–Goldburg homonuclear decoupling, resulted in a unique observation of intermolecular relationships across the host-guest interfaces.[13] The 2D ^1H–^{13}C spectra collected at a short contact time of 0.5 ms emphasized only the correlations of the hydrogen and carbon nuclei sitting at covalent bond distances, allowing the assignment of the PPS and PAN resonances (Figure 2c). In contrast, the 2D ^1H–^{13}C spectrum with a longer contact time exhibited new cross-peaks associated with intermolecular host-guest interactions that occurred through dipole-dipole interactions at short distances of less than 5 Å.

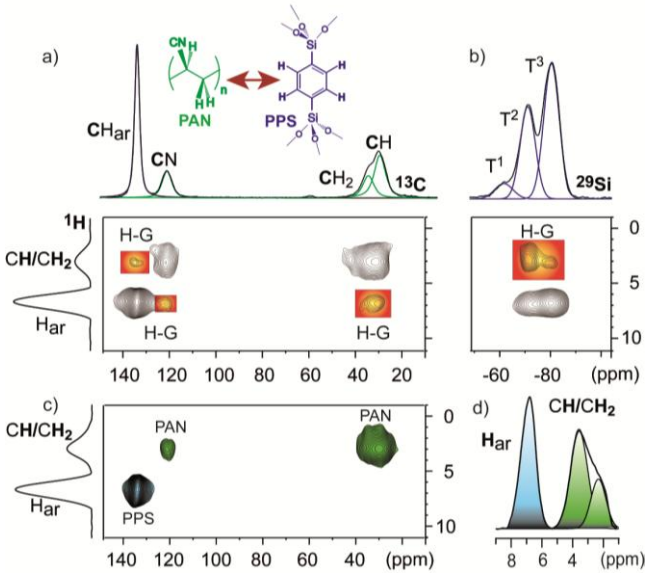

Figure 2. 2D ^1H-^{13}C and ^1H-^{29}Si HETCOR NMR spectra of PSS-PAN recorded by applying Phase Modulated Lee-Goldburg decoupling: (a) ^1H-^{13}C and (b) ^1H-^{29}Si spectra recorded by applying contact times of 5 and 8 ms, respectively. c) ^1H-^{13}C spectrum with a short contact time of 0.5 ms. In the carbon and silicon domains ^{13}C and ^{29}Si CP MAS spectra at 75.5 and 59.6 MHz are reported, respectively. Blue, green and orange cross-signals correspond to host-host, guest-guest and host-guest interactions, respectively. d) 600 MHz ^1H *w*PMLG MAS NMR spectrum of PPS-PAN. A spinning speed of 15 KHz was applied.

In Figure 2a, the cross-correlations that arise from the aromatic hydrogens of the host linker (δ_H=6.7 ppm) to the carbon nuclei of PAN guest (δ_{CN}, δ_{CH}, and δ_{CH2} at 121.1, 34.5 and 32.0 ppm) and from guest hydrogens ($\delta_H \cong 3$ ppm) to the host matrix (δ_C=134.0 ppm) are highlighted in orange. From an independent perspective,

the 2D ^{1}H-^{29}Si HETCOR spectrum showed the through space host-guest interactions. In fact, intense cross correlations between the guest aliphatic hydrogens and silicon atoms of the host siloxane groups (δ_{Si}=-71.3 and -80.6 ppm for T^2 and T^3 species of siloxane layers) were observed. These HETCOR NMR experiments bring to light a unique observation of the through-space communication at PPS-PAN interfaces, revealing the intimate relationship between host and guest moieties and the systematic insertion of aligned polymer bundles in the hybrid framework.

In the PPS-PAN nanocomposite the absence of polymer outside the mesochannels and the exclusive confinement of the polymer chains in the matrix was highlighted by calorimetric analysis. In fact, the DSC run at 10°C/min on PPS-PAN displayed an exotherm for the cyclization of PAN chains at lower temperature, beginning at 170°C and centered at 230°C, than in the reference bulk PAN[14] (Figure 3). The anticipated transformation temperature (40°C) is most likely due to the straight cylindrical nanochannels which impose an extended macroconformation to the included polymer chains and promote the intramolecular cyclization process. Additionally, the exotherm enthalpy provides the quantitative response of the confined polymer in the nanocomposite. The comparison between cyclization enthalpy of confined PAN (about 520 J/g, as normalized on the polymer content by TGA and MAS NMR) and that of pure PAN (550 J/g) suggested that PAN was completely transformed within the mesochannels. A second heating run on the same sample showed no exothermic phenomenon, indicating that the cyclization is an irreversible process.

In the PPS-PAN the presence of bulk PAN outside the nanochannels, which would produce a distinct narrow signal at 270°C, was ruled out and, in fact, such peak was only observed in samples containing excess PAN (PPS-*exc*PAN) (Figure 3c). Actually, polymerizations with excess monomer were performed systematically to construct nanocomposite materials containing PPS-PAN nanoparticles dispersed in a polymeric continuous phase. The interface interactions were ensured by polymer chains which participate in both the channels and the bulk and firmly anchor the polymer continuous phase to the porous network. It is worth noting that no reactants are needed to promote polymer–particle microadhesion, as frequently proven necessary with non-porous nanoparticles. Thus the sample containing excess PAN showed the possibility of constructing by a single polymerization step, a hierarchical architecture wherein the first-level nanocomposite, that is, PAN confined in porous PPS nanoparticles, is embedded in a polymer bulk forming the second level nanocomposite.

Collectively, the intramolecular cyclization process of confined PAN in PPS-PAN nanocomposite is an intriguing reaction that transforms the pristine polymer into the rigid ladder-like polymer in the nanospace. The first stage of the process involved the reaction of adjacent nitrile groups along the polymer chain, forming conjugated C=N unsaturations (Figure 3a). Additionally, C=C unsaturations involving the polymer main chain occur, forming a doubly polyconjugated polymer.[14] Conversely, the host mesoporous organosilica, which is highly stable up to 500°C, behaves as a chemical nanovessel for the thermally activated chemical reactions of PAN. Powder X-ray diffraction patterns of the nanocomposite after the thermal treatment at 300°C show no shift at either low or high 2Θ angles, demonstrating that the PAN thermal transformation into the ladder-polymer does not involve the host matrix at this stage.

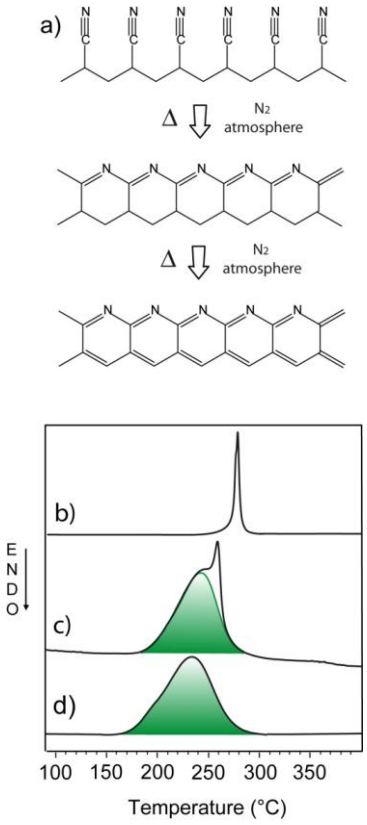

Figure 3. a) Chemical evolution of PAN by thermal treatment. DSC traces of pure PAN (b), PPS-*exc*PAN (c) and PPS-PAN (d). The green area corresponds to confined PAN exotherm.

The intramolecular cyclization process of confined PAN in PPS-PAN nanocomposite is an intriguing reaction that transforms the pristine polymer into the rigid ladder-like polymer in the nanospace. The first stage of the process involved the reaction of adjacent nitrile groups along the polymer chain, forming conjugated C=N unsaturations (Figure 3a). Additionally, C=C unsaturations involving the polymer main chain occur, forming a doubly polyconjugated polymer.[14] Conversely, the host mesoporous organosilica, which is highly stable up to 500°C, behaves as a chemical nanovessel for the thermally activated chemical reactions of PAN. Powder X-ray diffraction patterns of the nanocomposite after the thermal treatment at 300°C show no shift at either low or high 2Θ angles, demonstrating that the PAN thermal transformation into the ladder-polymer does not involve the host matrix at this stage.

The chemical transformation of PAN chains inside the mesochannels was followed by ^{13}C MAS NMR. In order to emphasize the evolution of the newly-formed chemical species involving the nitrile CN group, the in-situ polymerization in PPS matrix of ^{13}C- labelled acrylonitrile on CN moiety (20% enrichment) was performed (PPS-^{13}C-PAN nanocomposite). The ^{13}C CP MAS spectrum of the PPS-^{13}C-PAN, after thermal treatment at 300°C for 30 min, showed two main signals at δ= 149.9/153.0 ppm, diagnostic of isolated and conjugated C=N groups[14e] (Figure 4): the new

groups occurred at the expense of the nitrile CN (δ_C=121.5 ppm). The integral of C=N signals, as determined from the quantitative ^{13}C MAS NMR spectrum, indicates that about 82% of nitrile groups reacted and participated in the cyclization reaction. The C=C signals are hardly detected due to the selective labeling that shows only the carbons originated by the transformation of nitrile groups.

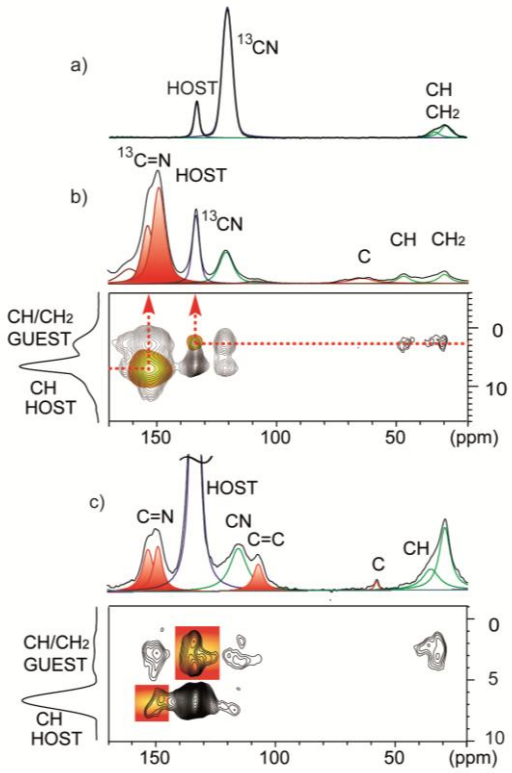

Figure 4. 1D and 2D MAS NMR spectra of the nanocomposite: a) ^{13}C CP MAS NMR spectrum of enriched-^{13}C PPS-PAN with 2 ms contact time. 2D ^{1}H-^{13}C NMR spectra with Phase Modulated Lee-Goldburg decoupling of b) enriched-^{13}C PPS-PAN and c) PPS-PAN. Both the samples underwent thermal treatment at 300°C. In the carbon and hydrogen domains the ^{13}C CP MAS and the ^{1}H projections are reported, respectively. The red peaks in the ^{13}C CP MAS spectra correspond to the newly-formed unsaturated species. Orange cross-signals correspond to host-guest interactions, respectively.

Thus, we recorded the ^{13}C CP MAS NMR spectrum of the PSS-PAN compound without ^{13}C-enriched carbons, which showed a comparable NMR response for all the carbon species. Actually, after thermal treatment at 300 °C for 2 hours, two intense and balanced signals for C=C and C=N unsaturation were observed (Figure 4c). The new unsaturated resonances were also recognized in the bulk-PAN ladder-structured polymer, demonstrating that the structural transformation of the PAN in matrix follows a similar reaction pathway.[14] The host resonance at δ_C=134.0 ppm is not affected by the thermal treatment, confirming that the matrix behaves at these temperatures as an inert nanoreactor for the chemical reaction involving the PAN macromolecules. Notably, 2D ^{1}H-^{13}C HETCOR MAS NMR experiments demonstrated the permanent confinement of the ladder polymer in the hybrid matrix: in fact, distinct cross-peaks between the host hydrogens at δ=6.7 ppm and ^{13}C-enriched C=N groups and *viceversa* from the guest hydrogens ($\delta_H \cong$ 3 ppm) to aromatic host carbons (δ_C=134.0 ppm) were observed, indicating a short distance communication between the ladder polymer formed *in situ* from PAN and the framework. This result clearly demonstrates the persistence of the intimate host-guest relationships among the components after curing, and the formation of an innovative material composed by two rigid structures: stiff and aligned polymer chains surrounded by a 3D framework.

After thermal treatment at 500°C of the PPS-PAN nanocomposite, the ^{13}C MAS NMR spectrum shows a decrease of C=N and C=C signal intensities and the disappearance of alifatic signals, indicating that further PAN evolution towards condensed aromatic species occurred (Supporting Information), whilst no significant change in the matrix aromatic units was observed. However, at such a high temperature the matrix starts modifying its connectivity: in fact, a small amount of the siloxane T^n species, associated with Si-C covalent bonds, transforms into a fully siliceous Q^n species, as demonstrated by the ^{29}Si MAS NMR spectrum (Supporting Information).

High temperature curing of the periodically ordered nanocomposite. Thermal transformations and structural evolution of PPS-PAN nanocomposite, as compared to the PPS empty matrix, was followed *in situ* by powder X-ray diffraction using a synchrotron radiation source (Figure 5).

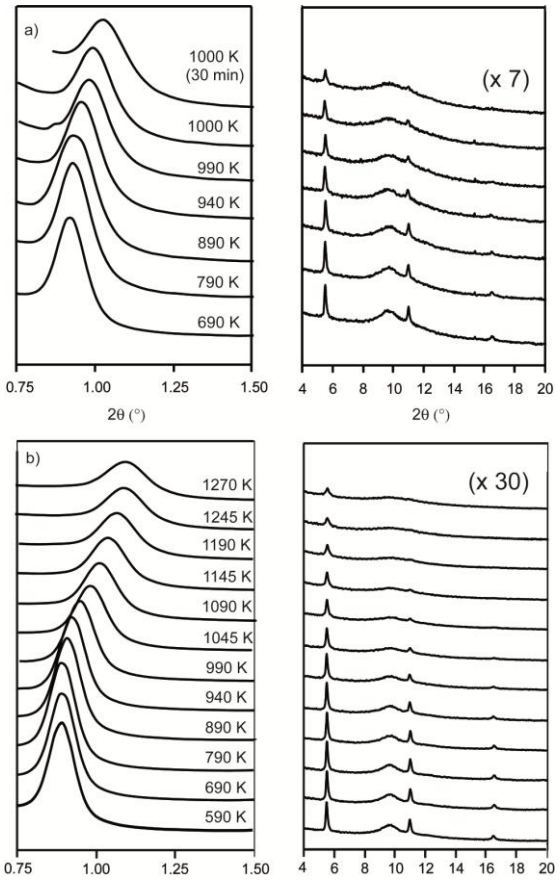

Figure 5. Powder X-ray diffraction patterns collected using synchrotron radiation of a) PPS-PAN nanocomposite and b) empty PPS at distinct temperatures. Low and high 2θ angles are shown in the left and right frames, respectively.

Synchrotron radiation, given its high energy beam and intense response, allowed us to efficiently follow in situ the evolution of the structures. Consequently, structural changes during heating was unveiled. The samples were put into a quartz capillary tube, which was heated with a scanning rate of 10 K/min under inert atmosphere. During the thermal treatment XRD patterns of PPS-PAN nanocomposite show a *d*-spacing value of 47.7 Å, associated with the mesopore order, that persists up to 800K. At higher temperatures a progressive shrinkage of the mesoscale peak was observed, reaching 37.7 Å after prolonged curing at 1000K for 30 min. Interestingly, the molecular order is still present at such high temperatures. The decrease at high temperature of the *d*-spacing led to 20% contraction of the lattice constant (a =43.5 Å) of the 2D hexagonal arrangement, consistent with a condensation process of the matrix aromatic moieties and the formation of polycyclic fused rings. A parallel behavior is observed in the empty PPS matrix (Figure 5b), although the nanocomposite shows a lower intensity, indicating that the nanochannels are occupied by polycyclic aromatic nanofibers as derived by PAN evolution.

Moreover, both the nanocomposite and the pure matrix were subjected to prolonged thermal treatment for several hours, at about 1350 K under argon atmosphere, yielding graphitic-like materials denoted as *g*-PPS-PAN and *g*-PPS, respectively. The N_2 adsorption isotherm of *g*-PPS showed a BET surface area of 633 m^2/g, with a reduced pore size of 26 Å, while in the *g*-PPS-PAN compound the absorption values were reduced by 5 times due to the carbon fibers that occupy the mesochannels (Figure 6). The TGA measurements, performed in air, indicated weight losses of 50% and 30% at 500°C for *g*-PPS-PAN and *g*-PPS, respectively, owing to the combustion of the reacted host-guest and pure host organic components, respectively. The occurrence of oxidative degradation at the same temperature in both compounds indicates that a common process occurred, unlike the untreated nanocomposite and pure matrix in which the thermal transformations followed distinct pathways.

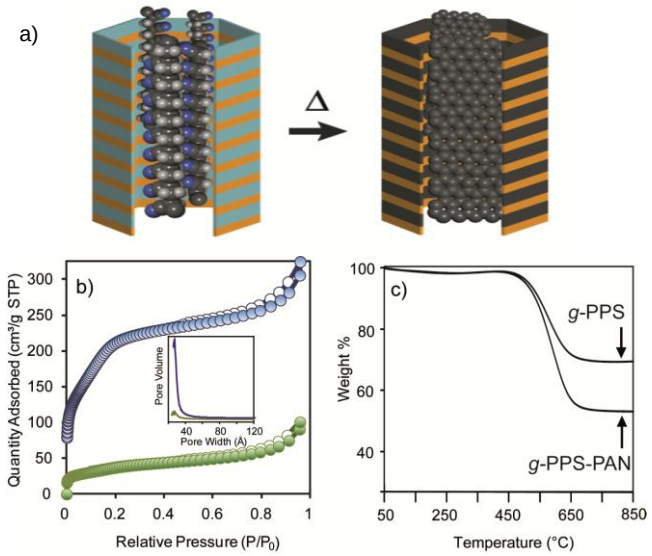

Figure 6. a) Schematic representation of thermal transformation of PPS-PAN to the graphitic-like structure. b) N_2 adsorption isotherms at 77K of *g*-PPS and *g*-PPS-PAN (highlighted in blue and green, respectively) and c) TGA analyses.

^{13}C MAS NMR of *g*-PPS-PAN revealed important features of the organic component transformation of both the polymer and the matrix, showing one resonance at δ_C=124 ppm, typical of graphitic-like structures[15] (Figure 7). No residual signals due to C=C and C=N groups, or aliphatic carbons, were observed. Also the matrix evolves to the aromatic-condensed structure: in fact, pristine *p*-phenylene moieties would yield a narrow signal at 134 ppm, which is absent in the ^{13}C MAS spectra of both the graphitic-like nanocomposite and the matrix (Supporting Information). The Raman spectrum of *g*-PPS/PAN reveals two peaks that represent typical features derived from graphitic-like structures.[16] The peaks at 1350 and 1600 cm^{-1} are associated with a breathing mode of graphitic carbon atoms (D peak) and an in-plane bond-stretching motion of the aromatic carbons (G peak), respectively. The D peak is not eliminated as in extended graphite because of the nanometric width of the organic domains obtained in the constrained geometries. A similar I(G)/I(D) ratio is due to the breaking of the translation symmetry of the graphite planes, as in the case of in-plane limited extensions of the domains in which the graphitic carbons become responsive to the domain borders.

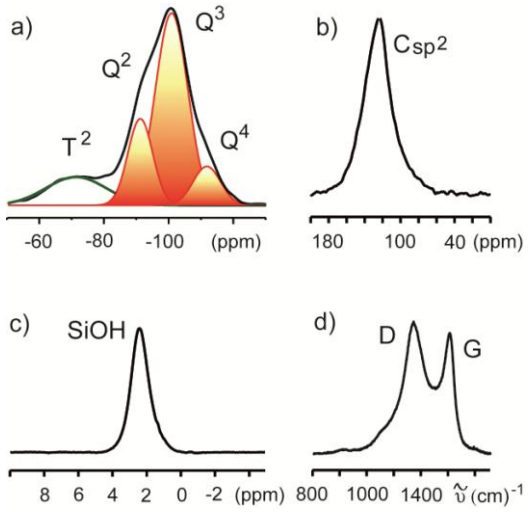

Figure 7. NMR and Raman spectroscopy of *g*-PPS-PAN: a) ^{29}Si CP MAS NMR recorded with a 8 ms contact time (chemical shifts of T^2, Q^2, Q^3 and Q^4 species at -71.5, -91.4, -101.1 and -112.0 ppm, respectively). b) ^{13}C MAS NMR performed with a 60 s recycle delay. c) High resolution 600 MHz ^1H MAS NMR spectrum (spinning speed of 30 KHz): the silanols resonate at δ^1H = 2.4 ppm. d) Raman spectrum: the typical D and G signals are indicated.

Significant structural changes induced in the siloxane-containing layers by the thermal treatment were observed by ^{29}Si MAS NMR spectroscopy: the spectrum of *g*-PPS-PAN displayed a major amount of Q^n groups (from -90 to -110 ppm) at the expense of the T^n species (δ_{Si}=-70 ppm), which are associated to organosilicon bonds (Figure 7a). This results in a dramatic change of the host connectivity involving the cleavage of C-Si bonds and the formation of siliceous species.[17] The silanol species, including geminal silanols (Q^2 and Q^3 units), prevail whilst the fully condensed Q^4 units, typical of conventional silica particles, are present in minor amount. Thus, the siloxane layers that anchor the *p*-phenylene

units in the pristine hybrid framework evolve after treatment into purely inorganic nanodomains constituted essentially by silanol species (Figure 7c). Silicon oxide structures composed exclusively by silanol Q^3 pertain to nanostructures confined to 2D layers, like fillosilicates, or nanoparticles with extremely low core-to-surface ratio.[18] An intriguing kind of carbon-silica nanocomposite was thus realized by in-situ generation of silica intimately interacting with a carbonaceous architecture. In particular, the novel nanostructured material is strenghtened by carbon nanofibers originated from PAN.

The powder X-ray pattern of *g*-PPS-PAN showed the disappearance of molecular order and a shrinkage of the mesoscale periodicity of more than 10 Å. The low intensity of the signal, as compared to *g*-PPS, indicates the homogenous distribution of electron density in the nanocomposite, confirming the embedding of polycyclic aromatic nanofibers in the restricted spaces provided by the mesochannels. The mesoscale order retention after treatment at such extreme temperatures was evident by direct observation of the contracted hexagonal structure using high-resolution TEM micrographs. The channel walls and the hexagonal shape of the single 'cells' can be appreciated with great clarity. A lateral view of the extended channels helped measure, once again, the channel diameter, and at the same time it gave an idea of the regularity of the novel nanostructures. Therefore, TEM images displayed the maintenance of the 2D hexagonal lattice and highlighted the hexagonal shape of the individual mesochannels even in the graphitic-like compound, indicating the formation of a robust material containing a periodically ordered matrix reinforced by carbon nanofibers. Finally, the removal of the inorganic component, carried out by HF, ended up with a fully carbonaceous material wherein the mesoscale order vanishes although the atomic scale layer-to-layer spacing of 3.4 Å witnesses the formation of nanometric graphitic-like structures.

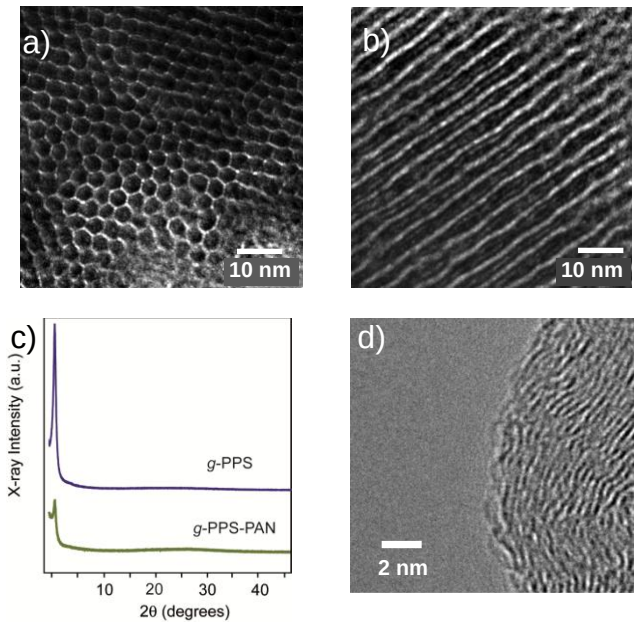

Figure 8. a) TEM images of g-PPS-PAN viewed along and perpendicular to the channel axis. c) Powder X-ray diffraction of *g*-PPS-PAN and *g*-PPS. d) HRTEM of HF etched *g*-PPS-PAN.

CONCLUSION

Confined polymerization of acrylonitrile in mesoporous *p*-phenylene organosilica was performed for the first time thanks to the open porosity of the periodically ordered architecture. This produced an unusual nanocomposite wherein a perfectly hexagonal honeycomb hybrid structure cooperates with nanometric bundles of high polymers to construct a sophisticated, yet ordered, texture. Moreover, the novel frameworks evolve with temperature, since both PAN and the aromatic channel walls are subjected to intra- and inter–molecular reactions. The intramolecular nitrile-group polymerization to yield a ladder polymer occurs with an anticipated exotherm and the newly formed chemical structures were recognized by 1D and 2D MAS NMR. Further reaction of the nanostructured material was followed *in situ* by synchrotron radiation X-ray diffraction up to high temperatures. A regular shrinkage of the hexagonal lattice from 5.5 to 4.3 nm, as observed by PXRD and high resolution TEM, demonstrated the notable persistence of order in the overall building up to 1350 K. This is clear evidence of aromatization of the *p*-phenylene moieties in the walls without a significant disrupture of the nanometric structure. Simultaneously, carbon-silicon covalent bonds of the matrix layered architecture are broken at such high temperatures, forming a hybrid carbon-silica nanocomposite wherein inorganic nanodomains of totally-oxydrylated silica cohabit with the condensed poly-aromatic framework reinforced by carbon nanofibers.

The intriguing variety of materials that could be created by this strategy to introduce carbon-nanofiber precursors, e.g. aromatic groups in the host matrix and confined polymer chains, and the possible cross reactions among the organic components makes it feasible to envisage new combinations of hybrid matrices and polymers to produce useful functions. In this particular case, we chose PAN as the target polymer as it is a well-known precursor of carbon fibers and graphitic-like materials. The present achievements show the extremely high degree of control enabled by the precise construction of porous materials with crystal-like order in their walls in combination with in-situ polymerization and polymer chemical transformations. The nanophase intimacy realized in the polymer-matrix ordered nanostructures and the perspective of a wide modulation of both the organic linker in the framework and the guest polymer make it feasible to conceive tailored architectures for light-harvesting and opto-electronic materials as well as in bio-medicine as controlled-released drug carriers.

ASSOCIATED CONTENT

Supporting Information. Solid State and solution NMR, calorimetric analyses, Raman spectra of the compounds are reported. This material is available free of charge via the Internet at http://pubs.acs.org.

AUTHOR INFORMATION

Corresponding Author

piero.sozzani@mater.unimib.it

Author Contributions

The manuscript was written through contributions of all authors. All authors have given approval to the final version of the manuscript.

ACKNOWLEDGMENT

The authors thank Prof. A. Paleari for the assistance in Raman measurements. Cariplo Foundation and PRIN 2012 are acknowledged for financial support.

REFERENCES

(1) (a) Uemura, T.; Yanai, N.; Kitagawa, S. *Chem.Soc.Rev.* **2009**, *38*, 1228–1236. (b) Tajima, K. ; Aida, T. *Chem. Commun.* **2000**, 2399–2412. (c) Comotti, A.; Bracco, S.; Mauri, M.; Mottadelli, S.; Ben, T.; Qiu, S.; Sozzani, P. *Angew. Chem. Int. Ed.* **2012**, *51*, 10136-10140. (d) Uemura, T.; Horike, S.; Kitagawa, K.; Mizuno, M.; Endo, K.; Bracco, S.; Comotti, A.; Sozzani, P.; Nagaoka, M.; Kitagawa, S. *J. Am. Chem. Soc.* **2008**, *130*, 6781–6788. (e) Sozzani, P.; Bracco, S.; Comotti, A.; Simonutti, R. *Adv. Polym. Sci.* **2005**, *181*, 153–177. (f) Lu, Y.; Yang, Y.; Sellinger, A.; Lu, M.; Huang, J.; Fan, H. ; Haddad, R.; Lopez, G.; Burns, A. R.; Sasaki, D. Y.; Shelnutt, J. ; Brinker, C. J. *Nature* **2001**, *410*, 913–917. (g) Kageyama, K.; Tamazawa, J.-I.; Aida, T. *Science* **1999**, *285*, 2113 –2115. (h) Wu, C. G.; Bein, T. *Science* **1994**, *266*, 1013–1015. (i) M. Farina, G. Di Silvestro, P. Sozzani in Comprehensive Supramolecular Chemistry, Vol. 6 (Ed.: J.-M. Lehn), Pergamon, Oxford, 1996, pp. 371 – 398; (l) M. Miyata, K. Sada in Comprehensive Supramolecular Chemistry, Vol. 6 (Ed.: J.-M. Lehn), Pergamon, Oxford, 1996, pp. 147 – 176; (m) Schilling, F. C.; Sozzani, P.; Bovey, F. A. *Macromolecules* **1991**, *24*, 4369–4375.

(2) (a) Distefano, G.; Suzuki, H.; Tsujimoto, M.; Isoda, S.; Bracco, S.; Comotti, A., Sozzani, P.; Uemura, T.; Kitagawa, S. *Nat. Chem.* **2013**, *5*, 335. (b) Distefano, G.; Comotti, A., Bracco, S.; Beretta, M.; Sozzani, P. *Angew. Chem. Int. Ed.* **2012**, *51*, 9258. (c) B. H. Jones, T. P. Lodge, *ACS Nano* **2011**, *5*, 8914–8927. (d) Yanai, N.; Uemura, T.; Ohba, M.; Kadowaki, Y.; Maesato, M.; Takenaka, M.; Nishitsuji, S.; Hasegawa, H.; Kitagawa, S.; *Angew. Chem. Int. Ed.* **2008**, *47*, 9883–9886. (e) Kazuki, S.; Masayuki, T.; Norifumi, F.; Numata, M.; Shinkai, S. *Chem.Soc.Rev.* **2007**, *36*, 415–435. (f) Choi, M.; Ryoo, R. *Nat. Mater.* **2003**, *2*, 473 – 476. (hg) Johnson, S. A.; Ollivier, P. J.; Mallouk, T. E. *Science* **1999**, *283*, 963 – 965.

(3) (a) Podsiadlo, P. ; Kaushik, A. K.; Arruda, E. M.; Waas, A. M.; Shim, B. S.; Xu, J.; Nandivada, H.; Pumplin, B. G.; Lahann, J.; Ramamoorthy, A.; Kotov, N. A. *Science* **2007**, *318*, 80–83. (b)Seema, A.; Kelarakis, A.; Estevez, L.; Giannelis, E. P. *Small* **2010**, *6*, 205–209. (c) Snyder, M. A.; Tsapatsis, M. *Angew. Chem. Int. Ed.* **2007**, *46*, 7560–7573. (d) Peng, H.; Sun, X.; Cai, F.; Chen, X.; Zhu, Y.; Liao, G.; Chen, D.; Li, Q.; Lu, Y.; Zhu, Y.; Jia, Q. *Nat. Nanotechnol.* **2009**, *4*, 738–741. (e) Yang Y. et al. *J. Am. Chem. Soc.* **2003**, *125*, 1269–1277. (f) Spange, S.; Grund, S. *Adv. Mater.* **2009**, *21*, 2111–2116. (g) Wang, Z.-M.; Wang, W. ; Coombs, N.; Soheilnia, N.; Ozin, G. A. *ACS Nano* **2010**, *4*, 7437–7450.

(4) (a) Liang, C.; Li, Z.; Dai, S. *Angew. Chem. Int. Ed.* **2008**, *47*, 3696-3717. (b) Lv, Y.; Wu, Z.; Fang, Y.; Qian, X.; Asiri, A. M.; Tu, B.; Zhao, D. *APL Mat.* **2014**, *2*, 113302-1-7. (c) Wu, Z. X.; Li, W. Xia, Y. Y.; Webley, P.; Zhao, D. Y. *J. Mater. Chem.* **2012**, *22*, 8835-8845. (d) Sozzani, P.; Bracco, S.; Comotti, A.; Simonutti, R.; Valsesia, P.; Sakamoto, Y.; Terasaki, O. *Nat. Mater.* **2006**, *5*, 545–551. (e) Valsesia, P.; Beretta, M.; Bracco, S.; Comotti, A. *J. Mater. Chem.* **2008**, *18*, 5511-5517. (f) Kruk, M.; Dufour, B., Celer, E. B.; Kowalewski, T.; Mietek, J.; Matyjaszewski , K. *J. Phys. Chem. B* **2005**, *109*, 9216-9225. (g) Lu, A.; Kiefer, A.; Schmidt, W.; Schüth, F. *Chem. Mater.* **2004**, *16*, 100-103. (h) Giunta, P. R.; Bossio, R. E.; Stiegman, A. E.; Marshall, A. G. *Chem. Mater.* **2003**, *15*, 1289-1295.

(5) (a) Hoffmann, F.; Froba, M. *Chem. Soc. Rev.* **2011**, *40*, 608-620. (b) Hoffmann, F.; Cornelius, M.; Morell, J.; Froba, M. *Angew. Chem. Int. Ed.* **2006**, *45*, 3216-3251.

(6) (a) Inagaki, S.; Guan, S.; Fukushima, Y.; Ohsuna, T.; Terasaki, O. *J. Am. Chem. Soc.* **1999**, *121*, 9611-9614. (b) Asefa, T.; MacLachlan, M. J.; Coombs, N.; Ozin, G. A. *Nature* **1999**, *402*, 867-871. (c) Melde, B. J.; Holland, B. T.; Blanford, C. F.; Stein, A. *Chem. Mater.* **1999**, *11*, 3302-3308.

(7) (a) Inagaki, S.; Guan, S.; Ohsuna, T.; Terasaki, O. *Nature* **2002**, *416*, 304-307. (b) Fujita, S.; Inagaki, S. *Chem. Mater.* **2008**, *20*, 891-908. (c) Mizoshita, N.; Tani, T.; Inagaki, S. Chem. Soc. Rev. **2011**, *40*, 789-800. (d) Kapoor, M. P.; Yang, Q.; Inagaki, S. *J. Am. Chem. Soc.* **2002**, *124*, 5176-15177. (e) Comotti, A.; Bracco, S.; Valsesia, P. Ferretti, L.; Sozzani, P. *J. Am. Chem. Soc.* **2007**, *129*, 8566-8576.

(8) (a) Sung Soo Park, S. S.; Moorthy, M. S.; Ha, C.-S. *NPG Asia Mater.* **2014**, *6*, e96-1- 21. (b) Mizoshita, N.; Goto, Y.; Tani, T.; Inagaki, S. *Adv. Mater.* **2009**, *21*, 4798-4801. (c) Waki, M.; Mizoshita, N.; Tani, T.; Inagaki, S. *Angew. Chem. Int. Ed.* **2011**, *50*, 11667-11671. (d) Maegawa, Y.; Mizoshita, N.; Tani, T.; Inagaki, S. *J. Mater. Chem.* **2010**, *20*, 4399-4403. (e) Goto, Y.; Ohsuna, T.; Mizoshita, N.; Tani, T.; Inagaki, S. *Solid State Sci.* **2011**, *13*, 729-735. (f) Shopsowitz, K. E.; Hamad, W. Y.; MacLachlan, M. J. *J. Am. Chem. Soc.* **2012**, *134*, 867-870. (g) Waki, M.; Mizoshita, N.; Maegawa, Y.; Hasegawa, T.; Tani, T.; Shimada, T.; Inagaki, S. *Chem. Eur. J.* **2012**, *18*, 1992-1998.

(9) (a) Park, M.; Park, S. S.; Selvaraj, M.; Kim, I.; Ha, C. S. *J. Porous Mater.* **2011**, *18*, 217. (b) Parambadath, S.; Rana, V. K.; Moorthy, S.; Chu, S. W.; Park, S. K.; Lee, D.; Sung, G.; Ha, C. S. *J. Solid State Chem.* **2011**, *184*, 1208. (c) Parambadath, S.; Rana, V. K.; Zhao, D. Y.; Ha, C. S. *Microp. Mesop. Mat.* **2011**, *141*, 94. (d) Shin, J. H.; Park, S. S.; Selvaraj, M.; Ha, C.-S. *J. Porous Mater.* **2010**, *19*, 29.

(10) Benson, K.; Prasetyanto, E. A.; Galla, H.-J.; Kehr, N. S. *Soft Matter* **2012**, *8*, 10845-10842.

(11) (a) Bracco, S.; Beretta, M.; Cattaneo, A.; Comotti, A.; Falqui, A.; Zhao, K.; Rogers, C.; Sozzani, P. *Angew. Chem. Int. Ed.* **2015**, *54*, 4773–4777. (b) Comotti, A.; Bracco, S.; Valsesia, P.; Beretta, M.; Sozzani, P. *Angew. Chem. Int. Ed.* **2010**, *49*, 1760-1764. (c) Bracco, S.; Comotti, A.; Valsesia, P.; Chmelka, B. F.; Sozzani, P. *Chem. Commun.* **2008**, 4798-4800. (d) Vogelsberg, C. S.; Bracco, S.; Beretta, M.; Comotti, A.; Sozzani, P.; Garcia-Garibay, M. A. *J. Phys. Chem. B* **2012**, *116*, 1623-1632.

(12) During the heating process, the intramolecular cyclization, aromatization and carbonization of PAN generated gas evolution, which consisted of a hydrogen and nitrogen-rich mixture.

(13) Vinogradov, E.; Madhu, P. K.; Vega, S. *J. Chem. Phys.* **2001**, *115*, 8983-9000. (b) Sozzani, P.; Comotti, A.; Bracco, S.; Simonutti, R. *Chem. Commun.* **2004**, 768-769. (c) Bracco, S. ; Comotti, A.; Ferretti, L.; Sozzani, P. *J. Am. Chem. Soc.* **2011**, *133*, 8982-8994. (d) Sozzani, P.; Bracco, S.; Comotti, A.; Simonutti, R.; Camurati, I. *J. Am. Chem. Soc.* **2003**, *125*, 12881-12893.

(14) (a) Fitzer, E. *Carbon* **1989**, *27*, 621- 645. (b) Ko, T. H. *J. Appl. Polym. Sci.* **1996**, *59*, 577 -580. (c) Rahaman, M. S. A.; Ismail, A. F.; Mustafa, A. A. *Polym. Degrad. Stab.* **2007**, *92*, 1421-1432. (d) Ruzimuradov, O.; Rajan, G. ; Mark, J. *Macromol. Symp.* **2006**, *245- 246*, 322-324. (e) Surianarayanan, M.; Vijayaraghavan, R.; Raghavan, K. V. *J. Polym. Sci. Part A: Polym. Chem.* **1998**, *36*, 2502-2512.

(15) (a) Si, Y.; Samulski, E. T. *Nanolett.* **2008**, *8*, 1679-1682. (b) Hiroyama, Y.; Kume, K. *Solid State Commun.* **1988**, *65*, 617-619. (c) Casabianca, L. B.; Shaibat, M. A.; Cai, W. W.; Park, S.; Piner, R.; Ruoff, R. S.; Ishii, Y. *J. Am. Chem. Soc.* **2010**, *132*, 5672-5676.

(16) (a) Cançado, L.G.; Takai, K.; Enoki, T.; Endo, M.; Kim, Y. A.; Mizusaki, H.; Jorio, A.; Coelho, L. N.; Magalhães-Paniago, R.; Pimenta, M. A. *Appl. Phys. Lett.* **2006**, *88*, 163106-1-3. (b) Ferrari, A. C. ; Robertson, J. *Phys. Rev. B* **2000**, *61*, 14095-14107.

(17) (a) Pang, J.; John, V. T.; Loy, D. A.; Yang, Z.; Lu, Y. Adv. Mater. 2005, 17, 704-707. (b)Legrand, A. P. *The surface properties of silicas*, Weinheim, Germany, Wiley (1998). (c) Faulkner, R. A.; DiVerdi, J. A.; Yang, Y.; Kobayashi, T.; Maciel, G. E. *Materials* **2013**, *6*, 18-46. (d) Sozzani, P.; Bracco, S.; Comotti, A.; Mauri, M.; Simonutti, R.; Valsesia, P. *Chem. Commun.* **2006**, 1921-1923. (e) Simonutti, R.; Comotti, A.; Bracco, S.; Sozzani, P. Chem. Mater. **2001**, *13*, 771-777. (f) Simonutti, R.; Comotti, A.; Sozzani, P.; Negroni, F. *Chem. Mater.* **1999**, *11*, 822-828.

SYNOPSIS TOC